ACS Catalysis

pubs.acs.org/acscatalysis Research Article

Effect of Oxygen–Iron Composition on Charge Transport and Interface Reaction in Hematite

Shuai Chen, Jiachen Wang, Mengyang Zhou, Hong Zhu, Yan Zhang, Jinhua Li,* Jing Bai, Ligang Xia, Qunjie Xu, and Baoxue Zhou*

Cite This: *ACS Catal.* 2020, 10, 2413–2418 Read Online

ACCESS | Metrics & More | Article Recommendations | Supporting Information

ABSTRACT: Hematite is composed of iron and oxygen elements, and the iron–oxygen spatial distribution would affect directly its photoelectrochemical (PEC) performance. However, less work has focused on the effect of iron–oxygen composition on the characteristic of charge transport and interfacial reaction. Here, we investigated the charge transfer and interface reaction of two typical iron–oxygen compositions of hematite prepared from the precursors of Fe and FeOOH in which different iron–oxygen ratios were obtained. X-ray photoelectron spectroscopy etching confirms that different precursors do cause differences in spatial elemental composition after thermal treatment. For Fe precursors, oxygen deficiency in the bulk is responsible for its lower bulk efficiency, whereas the defect-free surface results in a high surface separation efficiency and a low interfacial reaction catalysis rate. The FeOOH precursor forms an oxygen-rich surface and, therefore, introduces a large number of surface hole traps. Excessive traps significantly hinder surface charge separation and transport but favor surface electrocatalytic kinetics. Our work provides a perspective on the relationship between the semiconductor electrode performance and its structure and provides effective guidance for further optimization.

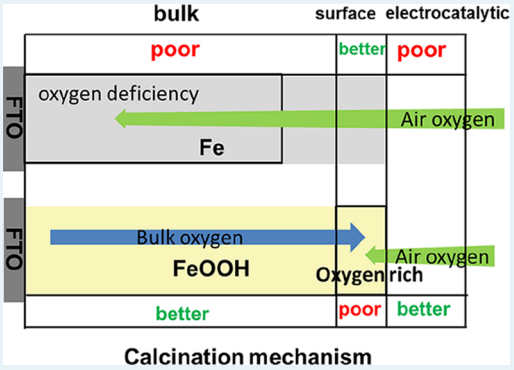

KEYWORDS: *hematite, iron–oxygen distribution, charge transfer, interface reaction, photoelectrochemistry*

INTRODUCTION

Hematite has been extensively studied as a photoanode for water decomposition.[1−8] So far, researchers have developed various preparation methods to enhance the PEC performance of hematite, such as classical hydrothermal method,[9−14] anodic and cathodic electrodeposition method,[15−17] direct thermal treatment method,[18] and so forth. Different preparation methods lead to different calcined precursors, which in turn result in differences in the spatial structure of the materials after thermal treatment (Fe–O ratio). These different iron–oxygen compositions are one of the root causes for the uneven PEC performance.[19] We have summarized these numerous preparation methods into two classic calcination precursors, Fe and FeOOH (note as ED-Fe_2O_3 and HT-Fe_2O_3 according to the preparation methods, electrodeposition and hydrothermal), which represent two different modes of oxygen diffusion during thermal treatment. For the former, the oxygen diffusion mechanism is relatively simple, that is, the oxygen in the air slowly diffuses into the interior of Fe at high temperature, forming a state in which the surface oxygen is sufficient and the internal oxygen is insufficient. Unlike Fe, FeOOH theoretically presents a more complex oxygen diffusion mechanism. On the one hand, the internal excess oxygen escapes to the surface in the form of water, and on the other hand, the oxygen in the air tends to diffuse into the interior at high temperature, together causing surface oxygen enrichment. Therefore, these two distinct diffusion mechanisms theoretically lead to completely different ratios of oxygen to iron on the vertical spatial scale (Figure 1a), affecting the PEC performance of the prepared hematite.

The spatial distribution of iron and oxygen will seriously affect the semiconductor bulk (conductivity, energy level position, and trap) and surface (trap, molecular adsorption, and interfacial reaction) properties. Different compositions of oxygen will also introduce functional sites, such as oxygen vacancies, which will make the effect of oxygen distribution on the semiconductor more confusing.[20,21] In addition, different distributions of oxygen can also serve as oxide semiconductor defects and further affect the bulk and surface quality.[20] Therefore, it is unreasonable to ignore these effects when analyzing the role of oxygen distribution in the PEC process. We thus use the hematite film electrode as our research object. In detail, we selected different calcination precursors as the research object under the same calcination conditions and

Received: October 21, 2019
Revised: January 15, 2020
Published: January 21, 2020

https://dx.doi.org/10.1021/acscatal.9b04538
ACS Catal. 2020, 10, 2413–2418

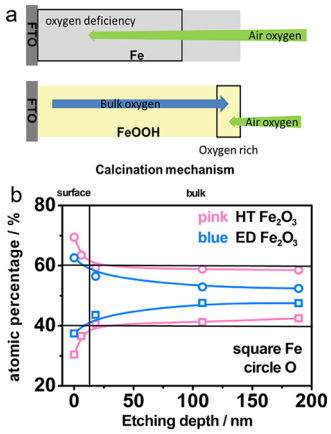

Figure 1. (a) Schematic illustration of oxygen diffusion mechanism of the electrodeposited Fe film and hydrothermal FeOOH film during calcination. (b) XPS etching spectra of ED-Fe_2O_3 and HT-Fe_2O_3.

investigated the oxygen content distribution by X-ray photoelectron spectroscopy (XPS) etching, and finally carefully study the effect of oxygen distribution on the charge transport and surface reaction of hematite through electrochemical tests.

RESULTS AND DISCUSSION

To this end, we prepared the Fe and FeOOH film calcined precursors by electrodeposition and hydrothermal methods, respectively, and calcined under the same conditions, showing a typical fine-grained compact morphology and wormlike nanorod arrays as shown in Figure S1 of the Supporting Information.[6,15] The X-ray diffraction (XRD) results confirm the formation of hematite phase mainly in the direction of (104) and (110) facets and a mere difference is observed between ED-Fe_2O_3 and HT-Fe_2O_3 (Figure S2, Supporting Information). Besides, the spatial scale relationship between oxygen and iron is detected by XPS etching, as shown in Figure 1b, confirming our previous speculation. For ED-Fe_2O_3, the oxygen in the air slowly diffuses into the interior of Fe during thermal treatment, forming a state that oxygen and iron reach the ratio of 3:2 only in the area near the surface, whereas the oxygen vacancy is widely distributed inside hematite (Figure 1). However, since the internal excess oxygen escapes to the surface in the form of water and the oxygen in the air tends to diffuse into the interior for HT-Fe_2O_3, it presents a completely different trend that oxygen and iron reach the ratio of 3:2 in the internal area whereas the surface state is oxygen-rich. That means the Fe/O ratio (surface of HT-Fe_2O_3 and bulk of ED-Fe_2O_3) will deviate from the stoichiometric ratio of hematite. Transmission electron microscopy elemental mapping proves that the surface element distribution of HT-Fe_2O_3 and ED-Fe_2O_3 is consistent with those measured by XPS etching (Figure S3, Supporting Information).

Opposite Charge-Transfer Mechanism. In this case, photocurrent densities of ED-Fe_2O_3 and HT-Fe_2O_3 were investigated in alkaline aqueous solution. Accordingly, almost equal photocurrent densities are obtained before 1.5 V_{RHE}, and this result meets the data in the reported literature (Figure S4a, Supporting Information). In addition, their incident photon-to-electron conversion efficiency (IPCE), applied bias photon-to-current efficiency (ABPE) and stability are also very close to each other (Figure S5, Supporting Information). However, the addition of a sacrificial agent (H_2O_2) significantly improves the photocurrent densities of HT-Fe_2O_3 rather than ED-Fe_2O_3, indicating the completely different internal charge-transfer mechanism. This was verified by the calculated bulk transfer efficiency (η_{bulk}) and surface charge injection efficiency ($\eta_{surface}$) as shown in Figure 2a and b where HT-Fe_2O_3 possess higher η_{bulk} and ED-Fe_2O_3 possess higher $\eta_{surface}$.

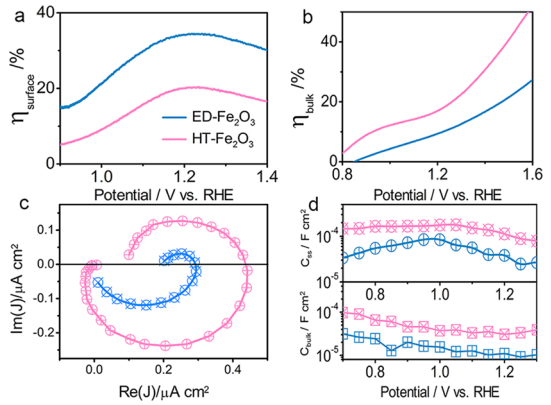

Figure 2. (a) Surface separation efficiency ($\eta_{surface}$) and (b) bulk separation efficiency (η_{bulk}) of ED-Fe_2O_3 and HT-Fe_2O_3. (c) IMPS of ED-Fe_2O_3 and HT-Fe_2O_3 measured at 1.23 V_{RHE}. (d) Surface state capacitance (C_{ss}) and bulk capacitance (C_{bulk}) obtained from EIS fitting for ED-Fe_2O_3 and HT-Fe_2O_3.

The intensity-modulated photocurrent spectrum (IMPS) and electrochemical impedance spectroscopy (EIS) tests also reflect the above conclusions (Figures 2c and S6, Supporting Information). As shown in Figure 2c, a significantly increased fourth quadrant capacitance−impedance arc indicates that more hole flux arrives at the surface, meaning better bulk carrier transfer of HT-Fe_2O_3. For ED-Fe_2O_3, a superior surface carrier transfer was observed (small first quadrant capacitance−impedance arc), although it featured poor bulk efficiency. In addition, we analyze the Nyquist plots (Figure S6a, Supporting Information) and perform the equivalent circuit diagram (Figure S6b, Supporting Information) fitting to obtain the fitting parameters of the corresponding components (Figure 2d). The bulk and surface capacitances of HT-Fe_2O_3 are both larger than those of ED-Fe_2O_3, which is exactly the same as the larger first and fourth quadrant arc of HT-Fe_2O_3 in IMPS results. Larger bulk (spatial charge layer) capacitance means greater hole flux, whereas larger surface capacitance is indicative of extremely complicated surface dynamics.

These diametrically opposite charge-transport performances of HT-Fe_2O_3 and ED-Fe_2O_3 are easily associated with their structural characteristics, that is, the more it deviates from the stoichiometric ratio of hematite (Fe/O ratio: 2:3), the lower the charge-transfer efficiency. Macroscopically, an n-type hematite semiconductor should exhibit a slightly oxygen-deficient structure to maintain its n-type features, just like the interior of HT-Fe_2O_3 and the area near the surface of ED-Fe_2O_3 (Figure 1). However, for the inside of ED-Fe_2O_3, a very low oxygen ratio leads to excessive solitary iron atoms, which will provide a lot of free electrons for the system, forming a large number of positive charge centers. These positive charge centers act as extremely serious bulk traps, capturing free electrons and further reducing the bulk charge-transport efficiency (Figure 3a). Similarly, the surface of HT-Fe_2O_3 has a large amount of solitary oxygen which captures the valence electrons from the surrounding iron atoms because of their strong electronegativity, forming the negative charge center at

https://dx.doi.org/10.1021/acscatal.9b04538
ACS Catal. 2020, 10, 2413−2418

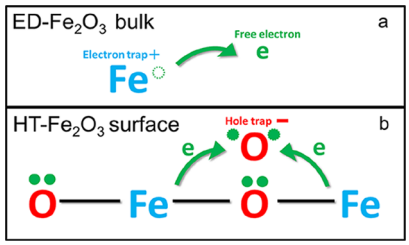

Figure 3. Schematic diagram of the formation mechanism for the (a) electron trap (interior of ED-Fe_2O_3) and (b) hole trap (surface of HT-Fe_2O_3). Hematite structure in (b) is a simplified connection way of iron atom and oxygen atom. (+) and (−) refer to the positive and negative charge centers, respectively. Dotted solid circle and dotted hollow circle refer to the trapped electrons on solitary oxygen atoms and formed holes on solitary iron atoms, respectively.

the position of solitary oxygen and acting as the hole trap (Figure 3b). The formation of a large number of hole traps makes the surface dynamics process of HT-Fe_2O_3 extremely complicated, which seriously reduces the surface charge-transport efficiency.

Surface Charge Transfer. Because of the critical role of the hematite surface trap dynamics process in the overall water oxidation process, the complex surface charge-transport process of the above HT-Fe_2O_3 will be the focus of our research. Transient-state photocurrent of HT-Fe_2O_3 and ED-Fe_2O_3 was measured under chopped illumination as shown in Figure 4a. Transient spikes were observed for HT-Fe_2O_3 when

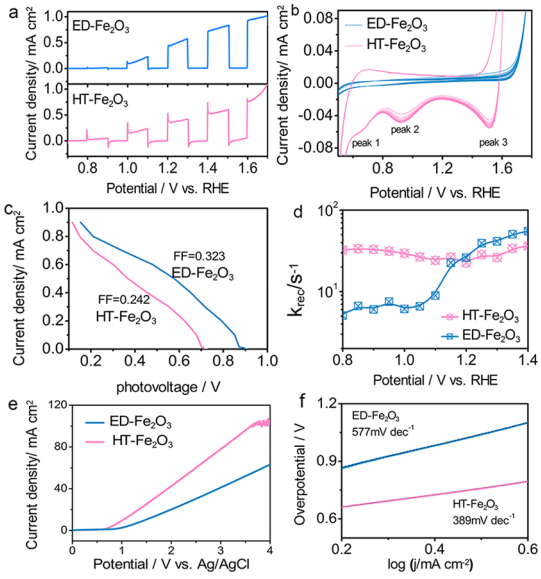

Figure 4. (a) Chopped linear sweep voltammograms, (b) CV measurement, (c) calculated photovoltaic performance at the semiconductor−electrolyte interface, (d) charge recombination rate constant (k_{rec}) obtained by EIS fitting, (e) current and voltage plots, and (f) Tafel plots of HT-Fe_2O_3 and ED-Fe_2O_3.

turning on the light, which is a typical feature of surface traps capturing holes (charging behavior of the trap capacitor).[22] This transient to steady-state process is accompanied by the decay of the non-Faradaic current (the hole is trapped by the surface trap) and the increase of the Faradaic current (the trapped hole gradually participates in the water oxidation reaction).[22,23] This indicates that for HT-Fe_2O_3, holes are transmitted to the surface at a very high speed under illumination and further quickly captured by surface traps to show the largest non-Faradaic current at the beginning. However, the trapped holes participating in water oxidation is a relatively slow process, and there is no excessive trap site to capture holes, resulting in a rapid decline in the non-Faradaic current.[24] During this process, the trapped holes gradually begin to participate in the water oxidation, eventually reaching the equilibrium of trapping and releasing holes in the trap dynamics. Only slight transient peaks were detected on ED-Fe_2O_3, indicating that the surface trap charging process of ED-Fe_2O_3 is very weak.

Then we further studied the surface-trapped hole site (oxidation state) by the cyclic voltammetry (CV) measurement. As shown in Figure 4b, three obvious reduction peaks located at 0.7, 0.95 , and 1.5 V_{RHE} are observed for HT-Fe_2O_3, whereas the CV curve of ED-Fe_2O_3 is very smooth without any reduction peak. This result implies that the surface of HT-Fe_2O_3 is enriched with a large amount of oxidizing substances (holes), in which the first peak could be ascribed to the oxygen p-hybridized states located close to the flat band,[25] the second peak is assigned to the reduction of water oxidation intermediates (water oxidation active site),[26] and the last severely accumulated reduction peak is the trap site where the hole is trapped and difficult to release,[27] possibly accompanied by a change in the chemical valence of iron.[8] Surface oxygen enrichment not only enhances beneficial traps (0.95 V_{RHE}) but also introduces a number of harmful traps (1.5 V_{RHE}), thus forming a surface-state capacitance value that is 1 order of magnitude more than that of ED-Fe_2O_3 (Figure 2c).

In addition, this wide-range surface traps significantly deteriorates the surface quality, as evidenced by the reduced open-circuit voltage (V_{oc}) and fill factor (FF) in Figure 4c, thus severely reducing the surface charge transport and separation efficiency.[20] At the same time, excessive trap distribution can also result in significant surface Fermi level pinning effects.[2] As shown in Figure 4a, the transient spike of HT-Fe_2O_3 does not change with the applied bias voltage and maintains a stable intensity of transient peak from 0.8 to 1.4 V_{RHE}, which is a significant feature of Fermi level pinning.[2] Moreover, the surface state capacitance (C_{ss}, Figure 2c) and the surface recombination constant (k_{rec}, Figure 4d) of HT-Fe_2O_3 do not change with the applied bias voltage (normal C_{ss} and K_{rec} should be Gaussian distributed or gradually increased with increasing bias voltage, respectively), indicating that HT-Fe_2O_3 is suffering from severe surface Fermi level pinning. These deleterious Fermi level pinning and decreased surface quality both cause surface charge retention and severe recombination.

Interface Reaction Mechanism. However, excessive surface oxygen trap distribution gives us a very beneficial advantage, namely excellent water oxidation active sites. As shown in Figure 4e, the onset potential of HT-Fe_2O_3 is lower than that of ED-Fe_2O_3, whereas the slope of the electrocatalytic current is much higher than that of the latter. Calculated by the Tafel curve illustrated in Figure 3f, the slope of HT-Fe_2O_3 is 389 mV dec^{-1}, which is smaller than that of ED-Fe_2O_3 (577 mV dec^{-1}), suggesting a superior surface reaction kinetics for HT-Fe_2O_3. Because the surface structure of ED-Fe_2O_3 conforms to the stoichiometric ratio of hematite, there are no excessive surface defects, and hence a large number of holes are directly transported to the surface from the valence band and participate in the water oxidation reaction. It is found through Figure 4e,f that this process is much slower, evincing that the valence band holes do not have

https://dx.doi.org/10.1021/acscatal.9b04538
ACS Catal. 2020, 10, 2413−2418

strong catalysis for hematite. As opposed to ED-Fe_2O_3, the majority of holes of HT-Fe_2O_3 are captured by surface traps and then involved in water oxidation, promoting the surface oxygen-rich trap site to become the water-reactive site in the Helmholtz layer. It turns out that the enrichment of this site greatly enhances the surface electrocatalytic water reaction kinetics. Similarly, the oxygen deficiency (oxygen vacancies) can also act as an excellent surface electrocatalytic active site.[20]

To further confirm the beneficial role of surface oxygen-rich trap site in the electrocatalytic water reaction, theoretical simulation was carried out on the (104) facet of hematite. In order to simulate the surface oxygen-rich environment of HT-Fe_2O_3, we constructed an appropriate amount of iron vacancy on the surface and used the unbonded oxygen surrounding the outermost iron vacancy as the adsorption site. The surface structure of ED-Fe_2O_3 is free of defects, and the bonded oxygen is treated as the adsorption site. After four steps of calculation, the free energy change is shown in Figure S7 of the Supporting Information. For ED-Fe_2O_3, the first step is undoubtedly the limiting step which needs a large amount of energy to form OOH*.[28] When the activated oxygen atom is used as a site (HT-Fe_2O_3), the free energy of this step is significantly decreased, indicating that HT-Fe_2O_3 is more conducive to the initiation of oxygen evolution reaction. In addition, since the single-step maximum free energy in the four-step reaction is significantly reduced (first step), the overpotential will also shrink, suggesting that the surface oxygen enrichment of HT-Fe_2O_3 does promote surface electrocatalytic oxygen evolution, in line with the above experimental results.[20]

Calcination Temperature Regulation. It is also well known that the oxygen diffusion process in semiconductors is very sensitive to temperature. To further verify the effect of the oxygen diffusion process on the semiconductor, we investigated the role of temperature changes on the PEC performance of as-prepared Fe and FeOOH. Because the normal calcination temperature for hematite is 700 °C in this work, we set the temperature change interval from 650 to 720 °C (650, 680, 700, and 720 °C). Through XPS etching, we found that the higher the temperature, the better the diffusion of oxygen in the air to the bulk phase, especially for ED-Fe_2O_3 (Figure S8, Supporting Information). This promotes a substantial increase in the bulk separation efficiency of ED-Fe_2O_3, which in turn increases its photocurrent density (Figure S9, Supporting Information). Furthermore, the high-temperature atmosphere is beneficial to the two-way diffusion process of oxygen in HT-Fe_2O_3, inducing that the surface is no longer the destination of oxygen accumulation. The decrease in surface oxygen concentration resulted in a significant decrease in the trap accumulation peak at 1.5 V_{RHE} and a significant increase in the photocurrent density in the plateau (Figure S10, Supporting Information). This indicates that the surface oxygen enrichment is directly related to the hole trap at 1.5 V_{RHE}, which seriously inhibits the growth of the plateau during the photocurrent after 1.23 V_{RHE}. Based on the results above, it is clear that the oxygen diffusion rate will have a huge impact on the semiconductor charge transport and PEC performance. In addition, we found that the performance of the sample calcined at 720 °C decreased because the high temperature caused the conductive glass to melt, resulting in a significant increase in the resistance of fluorine-doped tin oxide (FTO) (Figure S11, Supporting Information). However, this phenomenon is not representative, and the FTO of different manufacturing processes will withstand different temperatures.[25] Therefore, the 700° calcined sample is optimal herein.

By analyzing two types of oxygen diffusion semiconductors (Fe and FeOOH), we found that the PEC performance and charge-transport properties of semiconductor oxides are directly related to their oxygen−iron distribution. Although the morphologies of the two electrodes are quite different, their main physical features are similar (Figure S12, Supporting Information). Combined with its completely different chemical composition, we have reason to believe that the iron−oxygen distribution plays a major role in the charge transport of iron oxide in this work. When we do iron or oxygen doping modification on hematite, there is always an optimum concentration deviating from the stoichiometric ratio of hematite to achieve its optimal PEC performance. Thus, any change in the element exceeding the optimum concentration will become a harmful modification. In detail, the inner region of ED-Fe_2O_3 and the surface region of HT-Fe_2O_3 deviate significantly from the stoichiometric ratio of hematite, which becomes the limiting factor that hinders the increase in PEC performance. Basically, the carrier transfer occurred through three sequential steps after photoexcitation, including bulk carrier transfer, surface carrier transfer, and interface electrocatalytic process. In this case, although HT-Fe_2O_3 suffers from a poor surface charge-transport process, it possesses the same performance as ED-Fe_2O_3 because of its strong bulk transport and interfacial electrocatalytic performance. The surface oxygen-rich structure of HT-Fe_2O_3 deteriorates the surface quality, which can be used as an excellent electrocatalytic reaction site to promote the electrocatalytic process (Table S1). This brings us two inspirations: (i) As long as it is a metal oxide semiconductor, it will always involve the diffusion of oxygen during calcination. The samples calcined by different calcined precursors will be completely different. (ii) By analyzing the composition of the semiconductor, we can better perform precise modifications to improve the semiconductor performance.

■ ASSOCIATED CONTENT

Supporting Information

The Supporting Information is available free of charge at https://pubs.acs.org/doi/10.1021/acscatal.9b04538.

Scanning electron microscopy, XRD, photocurrent density, IPCE, APBE, EIS, equivalent circuits, calculated free energy, PEC performance of samples at different temperatures, and melting under high temperatures (PDF)

■ AUTHOR INFORMATION

Corresponding Authors

Jinhua Li − *School of Environmental Science and Engineering, Shanghai Jiao Tong University, Shanghai 200240, PR China*; Email: lijinhua@sjtu.edu.cn

Baoxue Zhou − *School of Environmental Science and Engineering, Shanghai Jiao Tong University, Shanghai 200240, PR China; Shanghai Institute of Pollution Control and Ecological Security, Shanghai 200092, P.R. China; Key Laboratory of Thin Film and Microfabrication Technology, Ministry of Education, Shanghai 200240, PR China;* orcid.org/0000-0001-6957-190X; Phone: (+86)21-54747351; Email: zhoubaoxue@sjtu.edu.cn; Fax: (+86)21-54747351

https://dx.doi.org/10.1021/acscatal.9b04538
ACS Catal. 2020, 10, 2413−2418

Authors

Shuai Chen − *School of Environmental Science and Engineering, Shanghai Jiao Tong University, Shanghai 200240, PR China*

Jiachen Wang − *School of Environmental Science and Engineering, Shanghai Jiao Tong University, Shanghai 200240, PR China*

Mengyang Zhou − *School of Environmental Science and Engineering, Shanghai Jiao Tong University, Shanghai 200240, PR China*

Hong Zhu − *University of Michigan-Shanghai Jiao Tong University Joint Institute, Shanghai Jiao Tong University, Shanghai 200240, PR China;* orcid.org/0000-0001-7919-5661

Yan Zhang − *School of Environmental Science and Engineering, Shanghai Jiao Tong University, Shanghai 200240, PR China*

Jing Bai − *School of Environmental Science and Engineering, Shanghai Jiao Tong University, Shanghai 200240, PR China*

Ligang Xia − *College of Environmental and Chemical Engineering, Shanghai University of Electric Power, Shanghai 200090, PR China; Shanghai Institute of Pollution Control and Ecological Security, Shanghai 200092, P.R. China*

Qunjie Xu − *College of Environmental and Chemical Engineering, Shanghai University of Electric Power, Shanghai 200090, PR China; Shanghai Institute of Pollution Control and Ecological Security, Shanghai 200092, P.R. China*

Complete contact information is available at: https://pubs.acs.org/10.1021/acscatal.9b04538

Notes

The authors declare no competing financial interest.

■ ACKNOWLEDGMENTS

The authors would like to acknowledge the National Key Research and Development Program of China (2018YFB1502001, 2018YFE0122300), Shanghai International Science and Technology Cooperation Fund Project (No. 18520744900), SJTU-AEMD and SJTU Center in High Performance Computing for support.

■ REFERENCES

(1) Tang, P.; Xie, H.; Ros, C.; Han, L.; Biset-Peiró, M.; He, Y.; Kramer, W.; Rodríguez, A. P.; Saucedo, E.; Galán-Mascarós, J. R.; Andreu, T.; Morante, J. R.; Arbiol, J. Enhanced photoelectrochemical water splitting of hematite multilayer nanowire photoanodes by tuning the surface state via bottom-up interfacial engineering. *Energy Environ. Sci.* **2017**, *10*, 2124−2136.

(2) Zhang, J.; García-Rodríguez, R.; Cameron, P.; Eslava, S. Role of cobalt−iron (oxy)hydroxide ($CoFeO_x$) as oxygen evolution catalyst on hematite photoanodes. *Energy Environ. Sci.* **2018**, *11*, 2972−2984.

(3) Deng, J.; Lv, X.; Liu, J.; Zhang, H.; Nie, K.; Hong, C.; Wang, J.; Sun, X.; Zhong, J.; Lee, S.-T. Thin-Layer Fe_2TiO_5 on Hematite for Efficient Solar Water Oxidation. *ACS Nano* **2015**, *9*, 5348.

(4) Ahn, H.-J.; Yoon, K.-Y.; Kwak, M.-J.; Park, J.; Jang, J.-H. Boron Doping of Metal-Doped Hematite for Reduced Surface Recombination in Water Splitting. *ACS Catal.* **2018**, *8*, 11932−11939.

(5) Chen, S.; Li, J.; Bai, J.; Xia, L.; Zhang, Y.; Li, L.; Xu, Q.; Zhou, B. Electron blocking and hole extraction by a dual-function layer for hematite with enhanced photoelectrocatalytic performance. *Appl. Catal., B* **2018**, *237*, 175−184.

(6) Jeon, T. H.; Moon, G.-h.; Park, H.; Choi, W. Ultra-efficient and durable photoelectrochemical water oxidation using elaborately designed hematite nanorod arrays. *Nano Energy* **2017**, *39*, 211−218.

(7) Liu, G.; Karuturi, S. K.; Chen, H.; Spiccia, L.; Tan, H. H.; Jagadish, C.; Wang, D.; Simonov, A. N.; Tricoli, A. Tuning the morphology and structure of disordered hematite photoanodes for improved water oxidation: A physical and chemical synergistic approach. *Nano Energy* **2018**, *53*, 745−752.

(8) Lin, H.; Long, X.; An, Y.; Zhou, D.; Yang, S. Three-Dimensional Decoupling Co-Catalyst from a Photoabsorbing Semiconductor as a New Strategy To Boost Photoelectrochemical Water Splitting. *Nano Lett.* **2018**, *19*, 455−460.

(9) Liao, A.; He, H.; Tang, L.; Li, Y.; Zhang, J.; Chen, J.; Chen, L.; Zhang, C.; Zhou, Y.; Zou, Z. Quasi-Topotactic Transformation of FeOOH Nanorods to Robust Fe_2O_3 Porous Nanopillars Triggered with a Facile Rapid Dehydration Strategy for Efficient Photoelectrochemical Water Splitting. *ACS Appl. Mater. Interfaces* **2018**, *10*, 10141−10146.

(10) Wang, J.; Wang, M.; Zhang, T.; Wang, Z.; Guo, P.; Su, J.; Guo, L. Facile Synthesis of Ultrafine Hematite Nanowire Arrays in Mixed Water-Ethanol-Acetic Acid Solution for Enhanced Charge Transport and Separation. *ACS Appl. Mater. Interfaces* **2018**, *10*, 12594−12602.

(11) Li, C.; Wang, T.; Luo, Z.; Liu, S.; Gong, J. Enhanced Charge Separation through ALD-Modified Fe_2O_3/Fe_2TiO_5Nanorod Heterojunction for Photoelectrochemical Water Oxidation. *Small* **2016**, *12*, 3415−3422.

(12) Jang, J.-W.; Du, C.; Ye, Y.; Lin, Y.; Yao, X.; Thorne, J.; Liu, E.; McMahon, G.; Zhu, J.; Javey, A.; Guo, J.; Wang, D. Enabling unassisted solar water splitting by iron oxide and silicon. *Nat. Commun.* **2015**, *6*, 7447−7451.

(13) Li, L.; Yu, Y.; Meng, F.; Tan, Y.; Hamers, R. J.; Jin, S. Facile solution synthesis of alpha-$FeF_3{\cdot}3H_2O$ nanowires and their conversion to α-Fe_2O_3 nanowires for photoelectrochemical application. *Nano Lett.* **2012**, *12*, 724−731.

(14) Li, M.; Yang, Y.; Ling, Y.; Qiu, W.; Wang, F.; Liu, T.; Song, Y.; Liu, X.; Fang, P.; Tong, Y.; Li, Y. Morphology and Doping Engineering of Sn-Doped Hematite Nanowire Photoanodes. *Nano Lett.* **2017**, *17*, 2490−2495.

(15) Zeng, Q.; Bai, J.; Li, J.; Xia, L.; Huang, K.; Li, X.; Zhou, B. A novel in situ preparation method for nanostructured α-Fe_2O_3 films from electrodeposited Fe films for efficient photoelectrocatalytic water splitting and the degradation of organic pollutants. *J. Mater. Chem. A* **2015**, *3*, 4345−4353.

(16) Zandi, O.; Schon, A. R.; Hajibabaei, H.; Hamann, T. W. Enhanced charge separation and collection in high-performance electrodeposited hematite films. *Chem. Mater.* **2016**, *28*, 765−771.

(17) Peerakiatkhajohn, P.; Yun, J.-H.; Chen, H.; Lyu, M.; Butburee, T.; Wang, L. Stable Hematite Nanosheet Photoanodes for Enhanced Photoelectrochemical Water Splitting. *Adv. Mater.* **2016**, *28*, 6405−6410.

(18) Grigorescu, S.; Lee, C.-Y.; Lee, K.; Albu, S.; Paramasivam, I.; Demetrescu, I.; Schmuki, P. Thermal air oxidation of Fe: rapid hematite nanowire growth and photoelectrochemical water splitting performance. *Electrochem. Commun.* **2012**, *23*, 59−62.

(19) Byun, S.; Jung, G.; Moon, S.-Y.; Kim, B.; Park, J. Y.; Jeon, S.; Nam, S.-W.; Shin, B. Compositional engineering of solution-processed $BiVO_4$ photoanodes toward highly efficient photoelectrochemical water oxidation. *Nano energy* **2018**, *43*, 244−252.

(20) Wang, Z.; Mao, X.; Chen, P.; Xiao, M.; Monny, S. A.; Wang, S.; Konarova, M.; Du, A.; Wang, L. Understanding the Roles of Oxygen Vacancies in Hematite-Based Photoelectrochemical Processes. *Angew. Chem., Int. Ed.* **2019**, *131*, 1042−1046.

(21) Liao, A.; Chen, R.; Fan, F.; Xiao, L.; He, H.; Zhang, C.; Asiri, A. M.; Zhou, Y.; Li, C.; Zou, Z. Integration of Fe_xS electrocatalysts and simultaneously generated interfacial oxygen vacancies to synergistically boost photoelectrochemical water splitting of Fe2O3 photoanodes. *Chem. Commun.* **2018**, *54*, 13817−13820.

(22) Klahr, B.; Gimenez, S.; Fabregat-Santiago, F.; Bisquert, J.; Hamann, T. W. Electrochemical and photoelectrochemical investigation of water oxidation with hematite electrodes. *Energy Environ. Sci.* **2012**, *5*, 7626−7636.

(23) Kim, D. W.; Riha, S. C.; DeMarco, E. J.; Martinson, A. B. F.; Farha, O. K.; Hupp, J. T. Greenlighting photoelectrochemical oxidation of water by iron oxide. *ACS Nano* **2014**, *8*, 12199−12207.

(24) Monllor-Satoca, D.; Bärtsch, M.; Fàbrega, C.; Genç, A.; Reinhard, S.; Andreu, T.; Arbiol, J.; Niederberger, M.; Morante, J. R. What do you do, titanium? Insight into the role of titanium oxide as a water oxidation promoter in hematite-based photoanodes. *Energy Environ. Sci.* **2015**, *8*, 3242−3254.
(25) Zandi, O.; Hamann, T. W. Enhanced Water Splitting Efficiency Through Selective Surface State Removal. *J. Phys. Chem. Lett.* **2014**, *5*, 1522−1526.
(26) Wang, Z.; Fan, F.; Wang, S.; Ding, C.; Zhao, Y.; Li, C. Bridging surface states and current−potential response over hematite-based photoelectrochemical water oxidation. *RSC Adv.* **2016**, *6*, 85582−85586.
(27) Cummings, C. Y.; Marken, F.; Peter, L. M.; Upul Wijayantha, K. G.; Tahir, A. A. New insights into water splitting at mesoporous α-Fe_2O_3 films: a study by modulated transmittance and impedance spectroscopies. *J. Am. Chem. Soc.* **2012**, *134*, 1228−1234.
(28) Iandolo, B.; Hellman, A. The role of surface States in the oxygen evolution reaction on hematite. *Angew. Chem., Int. Ed.* **2014**, *53*, 13404−13408.

https://dx.doi.org/10.1021/acscatal.9b04538
ACS Catal. 2020, 10, 2413−2418